RESEARCH ARTICLE | APRIL 03 2023

Moiré engineering in 2D heterostructures with process-induced strain Θ

Tara Peña ➡; Aditya Dey; Shoieb A. Chowdhury; ... et. al



Appl. Phys. Lett. 122, 143101 (2023) https://doi.org/10.1063/5.0142406





CrossMark

Articles You May Be Interested In

Ultrasonic delamination based adhesion testing for high-throughput assembly of van der Waals heterostructures

Journal of Applied Physics (December 2022)





Moiré engineering in 2D heterostructures with process-induced strain

Cite as: Appl. Phys. Lett. **122**, 143101 (2023); doi: 10.1063/5.0142406 Submitted: 13 January 2023 · Accepted: 19 March 2023 · Published Online: 3 April 2023







Tara Peña,^{1,a)} (b) Aditya Dey,² (b) Shoieb A. Chowdhury,² (b) Ahmad Azizimanesh,¹ (b) Wenhui Hou,¹ (b) Arfan Sewaket,¹ (b) Carla Watson,³ (b) Hesam Askari,² (b) and Stephen M. Wu^{1,3,a)} (b)

AFFILIATIONS

- 1 Department of Electrical and Computer Engineering, University of Rochester, Rochester, New York 14627, USA
- ²Department of Mechanical Engineering, University of Rochester, Rochester, New York 14627, USA
- ³Department of Physics and Astronomy, University of Rochester, Rochester, New York 14627, USA

ABSTRACT

We report deterministic control over a moiré superlattice interference pattern in twisted bilayer graphene by implementing designable device-level heterostrain with process-induced strain engineering, a widely used technique in industrial silicon nanofabrication processes. By depositing stressed thin films onto our twisted bilayer graphene samples, heterostrain magnitude and strain directionality can be controlled by stressor film force (film stress \times film thickness) and patterned stressor geometry, respectively. We examine strain and moiré interference with Raman spectroscopy through in-plane and moiré-activated phonon mode shifts. Results support systematic C_3 rotational symmetry breaking and tunable periodicity in moiré superlattices under the application of uniaxial or biaxial heterostrain. Experimental results are validated by molecular statics simulations and density functional theory based first principles calculations. This provides a method not only to tune moiré interference without additional twisting but also to allow for a systematic pathway to explore different van der Waals based moiré superlattice symmetries by deterministic design.

Published under an exclusive license by AIP Publishing. https://doi.org/10.1063/5.0142406

When heterostructures of stacked 2D van der Waals (vdW) materials are constructed with a relative twist between the layers, in-plane moiré interference patterns are created that vary in periodicity depending on angle. This in-plane superlattice effect can lead to the formation of flat-bands in twisted bilayer graphene (TBG) near a "magic-angle," which can cause strong electron interactions. Within this system alone, an amazing number of strongly correlated electronic phases appear that may be tuned by band filling. ^{1–6} Within the broader class of twisted vdW systems, including semiconducting transition metal dichalcogenides, there have also been reports of both similar electronic phases and strongly interacting optical phases. ^{7–12}

Significantly, these systems rely on the built-in moiré interference patterns formed only from twisting layers. The total space of possible moiré interference patterns is much larger when accounting for strain in each individual layer along with twist (Fig. 1). By individually straining one layer with respect to the other (heterostrain), substantial moiré tunability can be achieved. Specifically, biaxial or uniaxial heterostrain in twisted bilayer 2D heterostructures provides a pathway to manipulate the period of moiré interference [Fig. 1(b)] or change the geometry of the interference pattern [Fig. 1(d)]. Much of the correlated

electronic physics in twisted bilayer vdW systems can be understood in the framework of the Hubbard model with symmetry of the Hubbard lattice, the Coulomb repulsion (U), and hopping (t) terms all set by the twist angle alone. ^{13–15} A greatly expanded set of available lattice symmetries and direct control over U/t is possible with deterministic heterostrain in twisted bilayer 2D systems (Fig. 1), allowing an opportunity to better understand correlated electronic phases or serve as a basis for predicting new phases.

One key missing factor in exploring any of these concepts is the deterministic and continuous control of layer-by-layer strain, which has been lacking in the community studying twisted vdW moiré materials. Some works have explored the effects of applied heterostrain through probing uncontrollable heterostrain from fabrication processes, sengineered lattice mismatched epitaxial growth, and bending bilayers on flexible substrates, but there is a need for a general method compatible with all experimental probes and conditions. Systematic exploration of the strain-expanded phase space of 2D moiré quantum materials requires deterministic application of layer-by-layer strain on the device-level, compatible at low temperatures, with full control over uniaxiality vs biaxiality. Here, we present a

^{a)}Authors to whom correspondence should be addressed: tpena@ur.rochester.edu and stephen.wu@rochester.edu

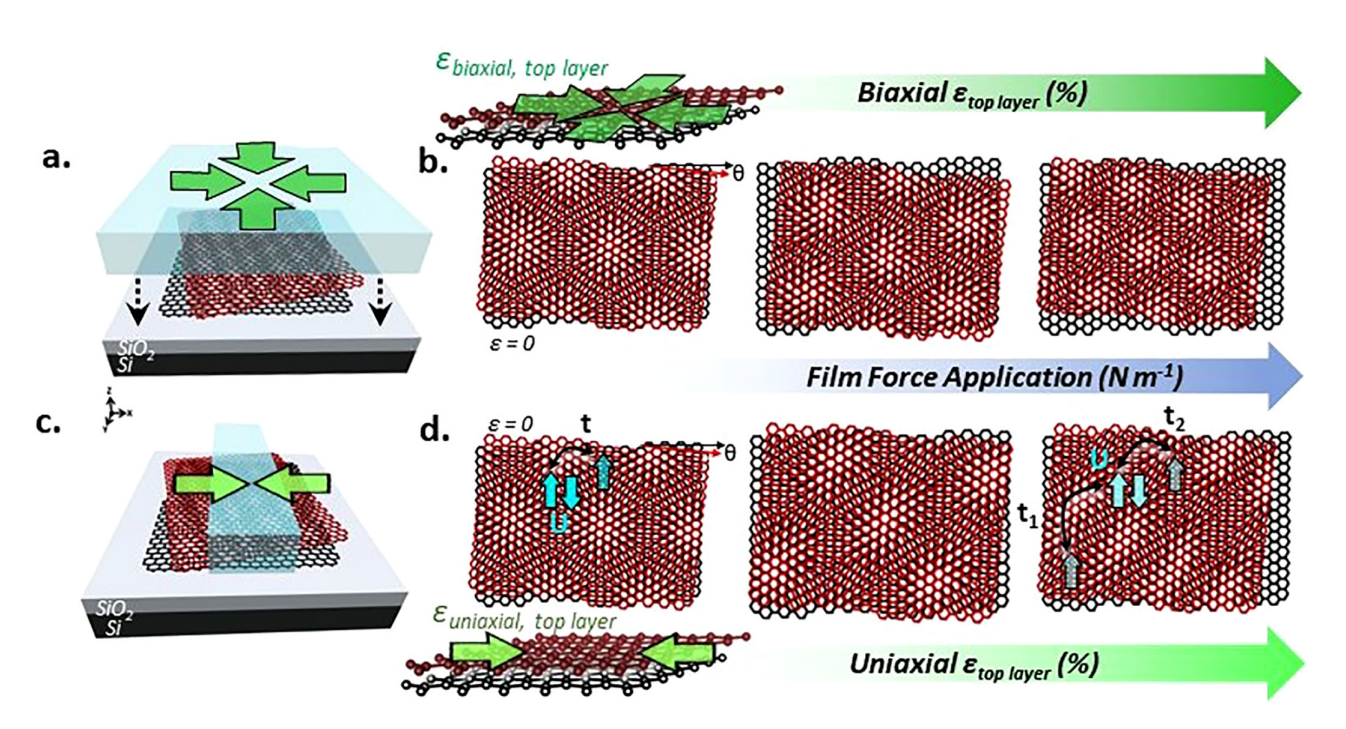


FIG. 1. (a) Highly stressed thin film fully encapsulating a TBG sample, providing biaxial strain to the top graphene layer. (b) Moiré interference pattern varying with biaxial heterostrain magnitude (rigid). (c) Highly stressed thin film patterned into a stripe on TBG, providing uniaxial strain to the top graphene layer (d) Moiré interference pattern varying with uniaxial heterostrain magnitude (rigid) and strain tunable Hubbard model parameters (blue).

method that meets all the above criteria with the deposition of highly stressed thin film capping layers (process-induced strain). We demonstrate that the heterostrain magnitude is directly proportional to the film force [film stress (GPa) \times film thickness (nm)] of the stressor layer, and strain directionality is controlled by the stressor geometry [Figs. 1(a) and 1(c)].

Process-induced strain engineering has been implemented in industrial silicon technology since the 90 nm technology node to selectively enhance electron or hole mobility in transistor channels. ^{21–23} In our previous work, this concept was proven to be equally versatile on vdW bonded 2D materials through evaporating highly stressed thin films onto various 2D multilayer flakes and heterostructures. ^{24–26} In these works, we show that process-induced strain can allow for the deterministic design over strain magnitude, tension or compression, uniaxiality or biaxiality, and strain direction relative to the crystal axes. ^{24,25} These methods when applied to 2D materials do not induce damage and are highly time stable and low-temperature compatible. ²⁶ Moreover, we also find incomplete out-of-plane strain transfer (heterostrain) naturally occurs in 2D structures from this method because of their weak vdW coupling, ²⁷ allowing for engineered layer-by-layer control over strain in 2D materials.

In this Letter, we apply process-induced strain to controllably heterostrain TBG structures to engineer the moiré periodicity and symmetry. Because bilayer graphene has weak interlayer coupling, we can strain the top graphene layer in this system, while the bottom layer is fixed to the substrate and entirely unstrained.^{24,28} This method is general to all 2D materials where substrate adhesion is higher than interlayer adhesion and can be integrated with complex device

structures on-chip, meeting all the criteria to examine these systems with low-temperature quantum transport experiments.

Raman spectroscopy is a popular, nondestructive method to extract details about strain, doping, and sample quality in 2D systems such as graphene and MoS₂. ^{29,30} Specifically, in high-angle TBG structures, an additional phonon mode is activated by the moiré superlattice, whose phonon frequency can be related back to the twist angle between the two monolayers [Figs. 2(a) and 2(b)].³¹ To understand this mode in TBG, one could look at the superlattice in reciprocal space, where two monolayer graphene Brillouin zones (BZs) are rotated by the given twist angle (θ) with respect to each other. The BZ of the moiré interference pattern (moiré-BZ) has reciprocal lattice vectors $\mathbf{q_1}$ and $\mathbf{q_2}$ [Fig. 2(c)], extracted from the difference between the monolayer reciprocal lattice vectors. The TBG's moiré activated phonon mode, termed as the R'(R) band, has a frequency dependent on the magnitude of vector $\mathbf{q}_{1,2}$. The R'(R) bands can be understood as the phonon dispersion curves along the Γ -K direction in bilayer graphene, where the longitudinal and transverse optical phonon branches (LO and TO) are active for twist angles below and above $\sim 10^{\circ}$, respectively [see supplementary material Fig. 2(b)]. 32,33 Since the vector $\mathbf{q}_{1,2}$ of the moiré-BZ is derived from the real-space superlattice vectors [Fig. 2(c)], this allows Raman analysis to provide information about strain-transfer and the subsequent real-space changes to the superlattice periodicity simultaneously in these structures. This is illustrated in Fig. 2(d), where biaxial heterostrain uniformly increases the magnitude of $q_{1,2}$, while uniaxial heterostrain increases and decreases both magnitudes of $\mathbf{q_1}$ and $\mathbf{q_2}$, respectively. This leads to the effects seen in R'(R)band manipulation by heterostrain in the following paragraphs.

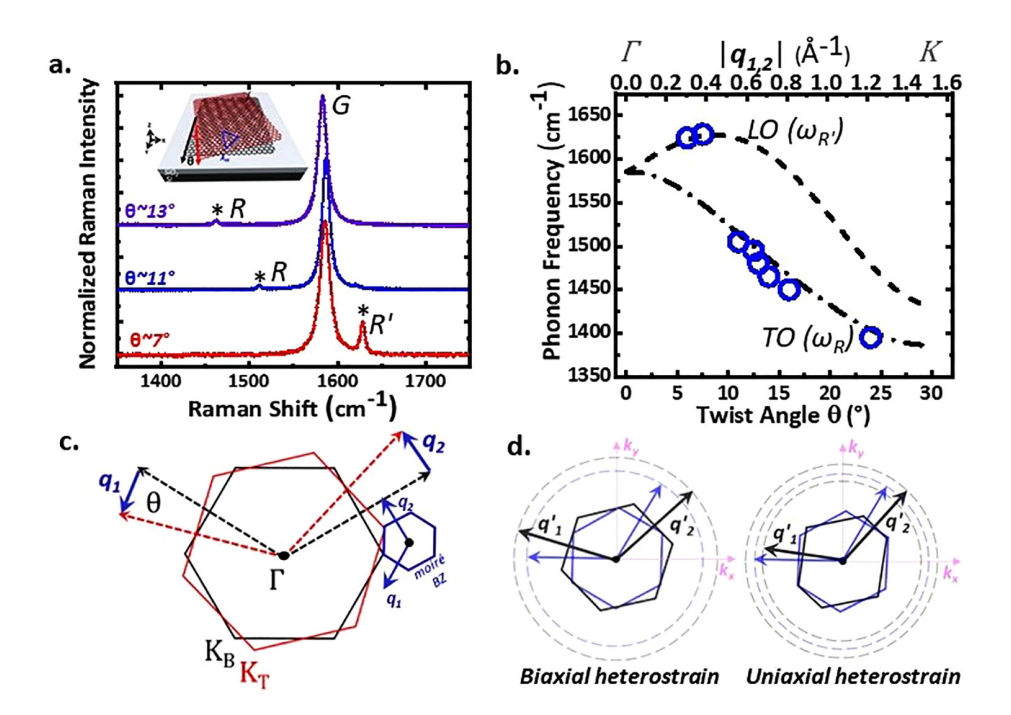


FIG. 2. (a) Raman spectra of TBG samples varying in the twist angle. (b) Phonon frequency of the moiré activated phonon mode with twist angle and q-vector magnitude. Open circles represent measured R/ R'-bands for various fabricated samples. (c) Brillouin zone schematic of unstrained twisted graphene monolayers (bottom—black, top—red) and the corresponding moiré Brillouin zone (blue). (d) Calculated moiré Brillouin zones under biaxial or uniaxial heterostrain (grey) compared to unstrained moiré Brillouin zones (blue).

We initially apply biaxial strain to the top layer in TBG structures (11° < θ < 16°, five TBG samples in total) and then probe changes in the in-plane (G-peak) and the superlattice phonon modes (R-peak) with increasing biaxial strain magnitude. Biaxial strain is expected since the thin film stressor would contract to relieve tensile stress from all directions, thus transferring biaxial strain to the top layer in contact with the stressor, as shown in our previous works. Raman spectroscopy is conducted on the TBG/SiO₂/Si sample before and after full encapsulation with a highly stressed tensile stressor (Fig. S1). The strain magnitude is directly proportional to thin film force application (N m⁻¹) of the stressor layer, and we choose to vary this parameter by varying the stressor thickness (see the supplementary material). Film force of the stressor layer is quantified via standard wafer curvature methods and then by employing the Stoney equation.

Since biaxial strain is being applied to the top graphene layer, the superlattice is expected to retain C₃ rotational symmetry, while the real-space moiré periodicity will decrease, and the magnitude of vector $\mathbf{q}_{1,2}$ will increase [Fig. 2(d)]. We quantify phonon shifts as the difference of pre- and post-encapsulation Raman peak positions $(\Delta\omega = \omega_{\text{after}} - \omega_{\text{before}})$, where we observe a redshift in the R-band and blueshift in the G-band in all samples after thin film stressor encapsulation [Fig. 3(a)]. The redshift in $\Delta\omega_R$ matches the expected increase in $|\mathbf{q}_{1,2}|$, and the blueshift in $\Delta\omega_{\rm G}$ confirms compressive strain transfer to the top graphene layer. Raman spectroscopic maps of the R-band peak positions before and after a 32 N m⁻¹ thin film force application on a TBG sample ($\theta \sim 14^{\circ}$) are shown in Figs. 3(b)-3(d), showing good uniformity of heterostrain application. Before encapsulation, the TBG sample displays an average R-band peak position of $1461.1 \pm 0.15 \,\mathrm{cm}^{-1}$. After the 32 N m⁻¹ encapsulation, we extract a new average R-band peak position of $1456.7 \pm 0.17 \,\mathrm{cm}^{-1}$. We repeat this procedure on four more TBG samples varying in film force application, where we find the magnitudes of both the R-band and G-band

shifts scale linearly with thin film force application [Figs. 3(e) and 3(f)], demonstrating direct controllability of heterostrain.

We next calculate the expected phonon frequency shifts with varying biaxial compressive strain magnitudes to the top graphene layer in a simulated 13.2° TBG using a combination of molecular statics (MS) and density functional theory (DFT) (see the supplementary material). Slopes of -30.48 and $10.21 \, \mathrm{cm}^{-1}/\%$ are obtained for $\Delta \omega_{\mathrm{R}}$ and $\Delta\omega_{\mathrm{G,top}}$ with applied strain, respectively, from these calculations. While a peak shift rate of 10.21 cm⁻¹/% for the G-band is smaller than literature values for biaxially strained graphene,³⁷ Raman shifts per % strain are unique to both the nature of the applied strain and to the 2D material structure itself. Because this is the only time biaxial heterostrain on TBG has been probed with Raman spectroscopy, we utilize our experimental peak shifts to validate and compare with our theoretical calculations. To independently compare experimental peak shifts as a function of strain, we estimate the % biaxial strain in the graphene top layer from film force alone. This is obtained by scaling our own result from biaxially strained monolayer MoS₂ (Ref. 24) by the relative elastic moduli between graphene and MoS2. Since graphene has a 3.5 times larger elastic modulus than MoS₂, the same film force will generate 3.5 times less strain. The experimental and calculated results are presented together in Figs. 3(e) and 3(f), where there is good agreement between measured peak shifts and simulated values. Thus, we have cross-verified that the biaxial heterostrain is being applied to TBG and this directly leads to modification of the moiré-BZ (periodicity) in the expected fashion. We do not expect to resolve the G-peak of each individual layer of graphene, because the G-peaks have much larger peak width (\sim 12 cm⁻¹) than this peak shift itself (\sim 2 cm⁻¹); however, we do observe this as an increase in the measured G-peak width of $\sim 0.65 \,\mathrm{cm}^{-1}$.

This good agreement between theory and experiment validates biaxial heterostrain as a mechanism to engineer the moiré wavelength,

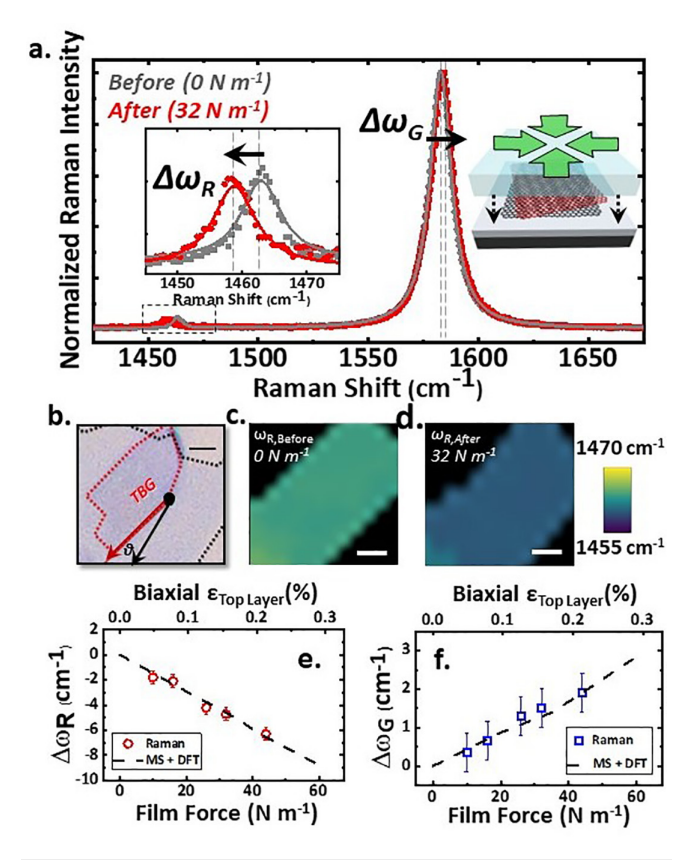


FIG. 3. Biaxial heterostrain case. (a) Raman spectra of a 14° TBG sample before and after a full encapsulation with a 32 N m⁻¹ thin film application. (b) Optical micrograph this TBG, scale bar is 1 μ m. Raman R-band peak position maps of this sample before (c) and after (d) the full encapsulation, scale bars are 0.5 μ m. Film force dependence of $\Delta\omega_{\rm R}$ (e) and $\Delta\omega_{\rm G}$ (f).

since R-band shifts can directly be mapped back to changes in $q_{1,2}$, and changes to $q_{1,2}$ represent changes to real-space moiré interference. These same real space modifications are observed through MS simulations and, subsequently, match experimental Raman results one-to-one [Figs. 3(e) and 3(f)]. Therefore, these results directly show a closed-loop theoretical/experimental approach to quantitatively engineer moiré periodicity, which is controlled continuously through biaxial heterostrain.

We now examine designed uniaxial heterostrain to TBG structures. Strain directionality (uniaxiality vs biaxiality) can be redefined by lithographically patterning the thin film stressors into stripes and modifying the width of the stripe. The uniaxial heterostrain is quite powerful particularly for moiré superlattices, because this type of strain can change the geometry of the moiré interference pattern from the typical triangular lattice to more complex patterns [Fig. 1(d)]. To explore this effect, we first lithographically pattern a 2.5 μm wide thin film stressor stripe (40 N m $^{-1}$) onto a 6° TBG sample [Fig. 4(b)], where the strain is determined to be uniaxial and perpendicular to the direction of the stripe (Fig S5), similar to our results in the previous work.

Prior to thin film stressor deposition, we confirm that the TBG sample displays uniform G and R' peak positions throughout the

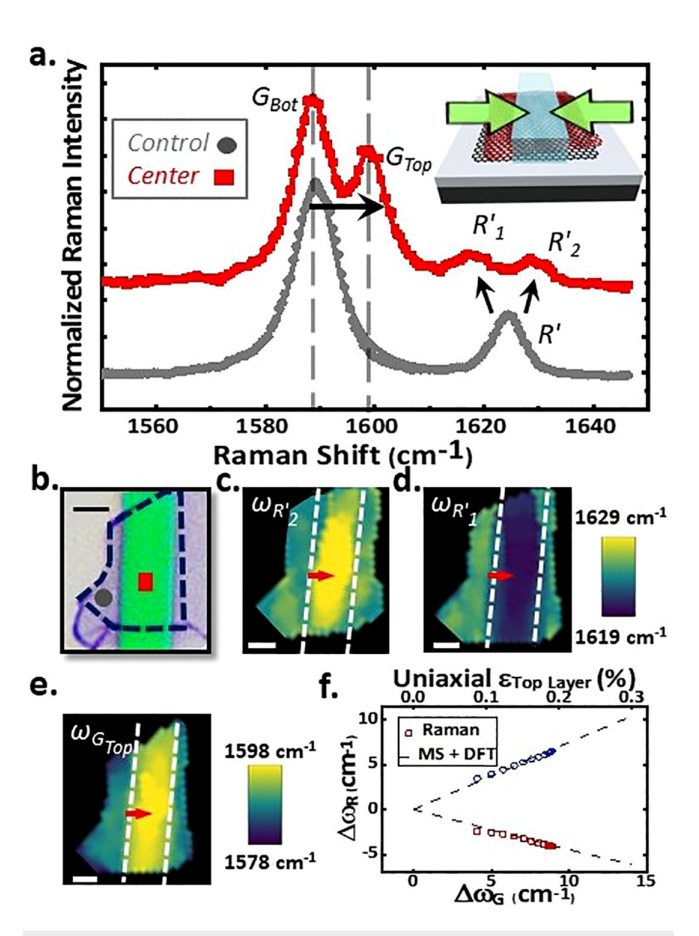


FIG. 4. Uniaxial heterostrain case. (a) Raman spectra outside the stressor and center of the stressor on a striped 6° TBG sample. (b) Optical micrograph of this TBG, scale bar is 2 μm . (c) and (d) Raman maps of R_1' and R_2' peak positions with the color bar placed to the right. (e) Raman maps of the G_{top} peak position with the color bar placed to the right. Raman maps have a 1 μm white scale bar. (f) $\Delta\omega_{R'1;R'2}$ as a function of $\Delta\omega_{\text{Glop}}$ taken from a line scan (red arrows of Raman maps).

sample (Fig. S3). After a 40 N m⁻¹ thin film stripe application, outside of the stressor displays the same G and R' positions as before the stressor deposition, then at the center of the stripe, we observe both G and R' peak splitting [Fig. 4(a)]. The G peak splitting in this sample arises from heterostrain, where each peak represents the G-peak of an individual layer. This is different than the typical G and G' $(E_{2\sigma}^+ \text{ and } E_{2\sigma}^-)$ peak splitting in individual graphene monolayers due to uniaxial strain that arises from lattice symmetry breaking, since we are well under the limit of strain magnitudes where this is a resolvable effect ($\varepsilon_{\text{uniaxial}} < 0.6\%$). The lower G-peak matches the unstrained (control) G-peak value in the TBG sample of \sim 1588.5 cm⁻¹, and, therefore, represents the signal from the unstrained bottom layer. The upper G-peak is blueshifted by $\sim 10.9 \, \mathrm{cm}^{-1}$, and we can estimate 0.21% compressive uniaxial strain to the top graphene layer when compensating for charge transfer contributions to the G-peak (Figs. S3 and S4). We can resolve G peak splitting from heterostrain in the uniaxial case (but not the biaxial case), because there is a larger Raman shift rate per % applied strain.

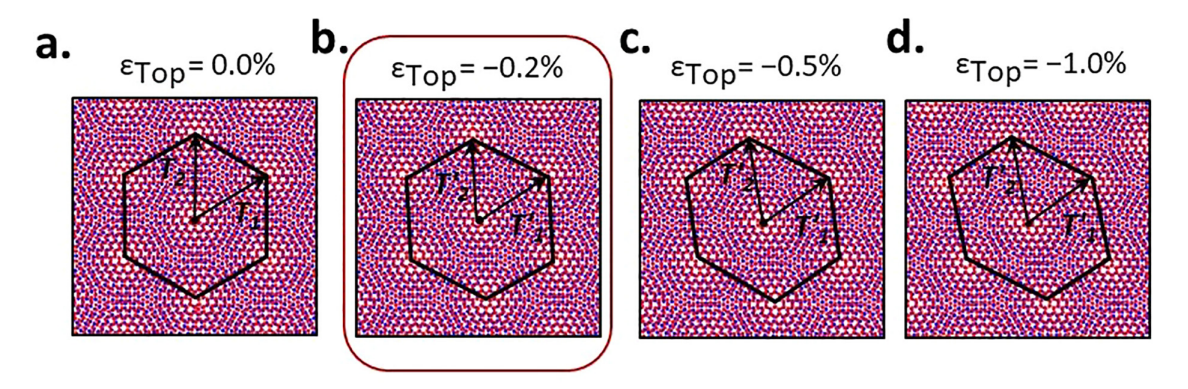


FIG. 5. Evolution of a moiré superlattice with applied uniaxial heterostrain. (a)–(d) Real-space MS captures of simulated 6° TBG samples varying with uniaxial compressive heterostrain magnitude applied along the zigzag direction.

While the G-peak splitting is due to contributions from each individual graphene layer, R'-peaks arise from the combined interaction between both graphene layers. Therefore, the splitting of this peak represents a direct modification to the moiré pattern itself. Under uniaxial heterostrain, we have shown that \mathbf{q}_1 and \mathbf{q}_2 vectors both increase and decrease in magnitude, arising from the breaking of the superlattice symmetry of unstrained or biaxially strained moiré interference [Figs. 1(d) and 2(d)]. Since the R' peak positions are directly related to the reciprocal space lattice vectors for the moiré-BZ (\mathbf{q}_1 , \mathbf{q}_2), this peak splitting represents direct evidence of C_3 rotational symmetry breaking in the moiré superlattice in TBG under deterministic application of uniaxial heterostrain. We have seen this as repeated across two other samples with patterned stressors and different film forces, where the G and R' peak splittings scale with film force application (Fig. S6).

To quantitatively confirm that the splitting and changes in $\omega_{R'}$ originate from changes in the moiré superlattice symmetry/periodicity, we also conduct Raman spectroscopic mapping over the entire sample [Fig. 4(b)]. When conducting Raman mapping, we observe clear correlations between both emerging R' peaks [Figs. 4(c) and 4(d)] and the G_{top} peak position [Fig. 4(e)]. Strain gradients are found at the edges of the thin film stressor [Figs. 4(c)-4(e) and Fig. S5(b)], indicating a full range of uniaxial heterostrain engineered by stressor geometry. To examine this more clearly, we plot the R' peak shifts as a function of G_{top} peak shifts [Fig. 4(f) symbols] and observe a one-to-one linear correlation between the Gtop and individual R' peak shifts, as expected from a full gradient of moiré interference patterns designed by uniaxial heterostrain within a single sample. We again calculate the phonon responses of a simulated heterostrained 6° TBG structure using MS+DFT to compare with our experimental data, where we find that the calculated phonon shifts match well to the experimental Raman data [dashed lines in Fig. 4(f)]. R' peak shifts per percent strain follow 34.83 and $-20.51 \, \text{cm}^{-1}$ /%, while the averaged G_{top} peak shift slope is 46.77 cm^{-1} /%.

Using our measured G_{top} and R' peak shifts, we can directly back-calculate the **exact** moiré-BZ and visualize the subsequent real-space moiré superlattice at the center of the stressor [Fig. 5(b)]. To illustrate the impact of uniaxial heterostrain application, we present the full evolution of MS+DFT simulated 6° TBG structures in real

space under increasing compressive uniaxial heterostrain magnitude from 0% to 1% (Fig. 5). Implementing a combined MS and DFT approach is critical to accurately account for atomic relaxation effects in the simulated heterostrained superlattices, ⁴⁰ allowing us to properly obtain the calculated phonon shifts with applied strain (see the supplementary material).

Here, we have introduced a method to locally engineer moiré periodicity and symmetry in 2D bilayer heterostructures by design. While this demonstration implemented ~0.2% heterostrain on TBG, this does not represent an upper limit to the amount of strain that can be applied by our method. Several other theoretical and experimental works suggest that ~0.2% heterostrain is already enough to substantially modify the moiré periodicity and, subsequently, alter the electronic properties in systems like magic-angle TBG. 18,19,41-44 Moreover, we have engineered other 2D systems up to 0.85%, ²⁴ with more recent results even reaching 1.5%. The heterostrain applied by process induced strain engineering is general and can be continuously tuned by varying thin film force application and thin film stressor geometry. These heterostrain modifications allow for controlled access to moiré interference patterns that are not achievable through twist alone. Our combined experimental and theoretical approach allows for direct inference of the real space moiré modifications made through heterostrain, allowing for direct quantitative back calculation of the engineered moiré patterns from Raman spectroscopic analysis. This closed-loop approach allows for systematic engineering of moiré interference in bilayer 2D heterostructures that has not been achieved deterministically before, opening the door to a strain-expanded exploration of twisted 2D quantum materials by design.

See the supplementary material for the details on the MS simulations, DFT calculations, and experimental Raman methods and also for the details of methods of sample preparation, fabrication, and characterization; quantifying charge transfer from the thermally evaporated thin film stressor layer (Fig. S1); quantifying charge transfer from this multilayer e-beam evaporated stressor (Fig. S2); Raman maps of the 6° TBG sample before photolithography and stressor deposition (Fig. S3); estimating the G-peak shift from strain alone with the e-beam multilayer stressor (Fig. S4); polarization-dependent Raman results and high-resolution line scan over the striped 6° TBG sample (Fig. S5); Raman spectra of a

7° TBG sample before and after the patterned thermally evaporated stressor (Fig. S6); and time stability of strain and moiré periodicity on the striped 6° TBG sample (Fig. S7).

We acknowledge support from the National Science Foundation (NSF) (Nos. OMA-1936250 and ECCS-1942815) and the National Science Foundation Graduate Research Fellowship Program (No. DGE-1939268). Raman spectroscopy was performed at the Cornell Center for Materials Research Shared Facilities (CCMR), and CCMR is supported through the NSF MRSEC Program (No. DMR-1719875).

AUTHOR DECLARATIONS Conflict of Interest

The authors have no conflicts to disclose.

Author Contributions

Tara Peña: Conceptualization (equal); Data curation (equal); Formal analysis (equal); Investigation (equal); Methodology (equal); Writing – original draft (equal); Writing – review & editing (equal). Aditya Dey: Data curation (equal); Formal analysis (equal); Investigation (equal); Methodology (equal); Writing – original draft (equal); Writing – review & editing (equal). Shoieb A. Chowdhury: Data curation (equal); Investigation (equal); Writing – review & editing (equal). Ahmad Azizimanesh: Investigation (equal). Wenhui Hou: Investigation (equal). Arfan Sewaket: Investigation (equal). Carla Watson: Investigation (equal). Hesam Askari: Funding acquisition (equal); Investigation (equal); Supervision (equal); Validation (equal); Writing – review & editing (equal). Stephen Mingda Wu: Conceptualization (equal); Funding acquisition (equal); Investigation (equal); Project administration (equal); Supervision (equal); Validation (equal); Writing – original draft (equal); Writing – review & editing (equal).

DATA AVAILABILITY

The data that support the findings of this study are available from the corresponding authors upon reasonable request.

REFERENCES

- ¹Y. Cao, V. Fatemi, S. Fang, K. Watanabe, T. Taniguchi, E. Kaxiras, and P. Jarillo-Herrero, "Unconventional superconductivity in magic-angle graphene superlattices," Nature 556, 43–50 (2018).
- ²Y. Cao, V. Fatemi, A. Demir, S. Fang, S. L. Tomarken, J. Y. Luo, J. D. Sanchez-Yamagishi, K. Watanabe, T. Taniguchi, E. Kaxiras, R. C. Ashoori, and P. Jarillo-Herrero, "Correlated insulator behaviour at half-filling in magic-angle graphene superlattices," Nature 556, 80–84 (2018).
- graphene superlattices," Nature 556, 80–84 (2018).

 3H. Polshyn, J. Zhu, M. A. Kumar, Y. Zhang, F. Yang, C. L. Tschirhart, M. Serlin, K. Watanabe, T. Taniguchi, A. H. MacDonald, and A. F. Young, "Electrical switching of magnetic order in an orbital Chern insulator," Nature 588, 66–70 (2020).
- ⁴A. L. Sharpe, E. J. Fox, A. W. Barnard, J. Finney, K. Watanabe, T. Taniguchi, M. A. Kastner, and D. Goldhaber-Gordon, "Emergent ferromagnetism near three-quarters filling in twisted bilayer graphene," Science 365, 605–608 (2019).
- 5M. Serlin, C. L. Tschirhart, H. Polshyn, Y. Zhang, J. Zhu, K. Watanabe, T. Taniguchi, L. Balents, and A. F. Young, "Intrinsic quantized anomalous Hall effect in a moiré heterostructure," Science 367, 900–903 (2020).
- ⁶Y. Choi, H. Kim, Y. Peng, A. Thomson, C. Lewandowski, R. Polski, Y. Zhang, H. S. Arora, K. Watanabe, T. Taniguchi, J. Alicea, and S. Nadj-Perge,

- "Correlation-driven topological phases in magic-angle twisted bilayer graphene," Nature 589, 536–541 (2021).
- ⁷Z. Zhang, Y. Wang, K. Watanabe, T. Taniguchi, K. Ueno, E. Tutuc, and B. J. LeRoy, "Flat bands in twisted bilayer transition metal dichalcogenides," Nat. Phys. 16, 1093–1096 (2020).
- ⁸L. Wang, E. M. Shih, A. Ghiotto, L. Xian, D. A. Rhodes, C. Tan, M. Claassen, D. M. Kennes, Y. Bai, B. Kim, K. Watanabe, T. Taniguchi, X. Zhu, J. Hone, A. Rubio, A. N. Pasupathy, and C. R. Dean, "Correlated electronic phases in twisted bilayer transition metal dichalcogenides," Nat. Mater. 19, 861–866 (2020).
- ⁹T. Li, S. Jiang, L. Li, Y. Zhang, K. Kang, J. Zhu, K. Watanabe, T. Taniguchi, D. Chowdhury, L. Fu, J. Shan, and K. F. Mak, "Continuous Mott transition in semiconductor moiré superlattices," Nature 597, 350–354 (2021).
- ¹⁰C. Jin, E. C. Regan, A. Yan, M. Iqbal Bakti Utama, D. Wang, S. Zhao, Y. Qin, S. Yang, Z. Zheng, S. Shi, K. Watanabe, T. Taniguchi, S. Tongay, A. Zettl, and F. Wang, "Observation of moiré excitons in WSe₂/WS₂ heterostructure superlattices," Nature 567, 76–80 (2019).
- ¹¹Y. Xu, S. Liu, D. A. Rhodes, K. Watanabe, T. Taniguchi, J. Hone, V. Elser, K. F. Mak, and J. Shan, "Correlated insulating states at fractional fillings of moiré superlattices," Nature 587, 214–218 (2020).
- ¹²K. Tran, G. Moody, F. Wu, X. Lu, J. Choi, K. Kim, A. Rai, D. A. Sanchez, J. Quan, A. Singh, J. Embley, A. Zepeda, M. Campbell, T. Autry, T. Taniguchi, K. Watanabe, N. Lu, S. K. Banerjee, K. L. Silverman, S. Kim, E. Tutuc, L. Yang, A. H. MacDonald, and X. Li, "Evidence for moiré excitons in van der Waals heterostructures," Nature 567, 71–75 (2019).
- ¹³N. F. Q. Yuan and L. Fu, "Model for the metal-insulator transition in graphene superlattices and beyond," Phys. Rev. B 98, 045103 (2018).
- ¹⁴M. Koshino, N. F. Q. Yuan, T. Koretsune, M. Ochi, K. Kuroki, and L. Fu, "Maximally localized Wannier orbitals and the extended Hubbard model for twisted bilayer graphene," Phys. Rev. X 8, 031087 (2018).
- ¹⁵F. Wu, T. Lovorn, E. Tutuc, and A. H. Macdonald, "Hubbard model physics in transition metal dichalcogenide moiré bands," Phys. Rev. Lett. 121, 026402 (2018).
- ¹⁶E. Y. Andrei, D. K. Efetov, P. Jarillo-Herrero, A. H. MacDonald, K. F. Mak, T. Senthil, E. Tutuc, A. Yazdani, and A. F. Young, "The marvels of moiré materials," Nat. Rev. Mater. 6, 201–206 (2021).
- 17C. N. Lau, M. W. Bockrath, K. F. Mak, and F. Zhang, "Reproducibility in the fabrication and physics of moiré materials," Nature 602, 41–50 (2022).
- ¹⁸N. P. Kazmierczak, M. Van Winkle, C. Ophus, K. C. Bustillo, S. Carr, H. G. Brown, J. Ciston, T. Taniguchi, K. Watanabe, and D. K. Bediako, "Strain fields in twisted bilayer graphene," Nat. Mater. 20, 956–963 (2021).
- 19J.-B. Qiao, L.-J. Yin, and L. He, "Twisted graphene bilayer around the first magic angle engineered by heterostrain," Phys. Rev. B 98, 235402 (2018).
- ²⁰X. Gao, H. Sun, D.-H. Kang, C. Wang, Q. J. Wang, and D. Nam, "Heterostrain-enabled dynamically tunable moiré superlattice in twisted bilayer graphene," Sci. Rep. 11, 21402 (2021).
- ²¹S. E. Thompson, M. Armstrong, C. Auth, M. Alavi, M. Buehler, R. Chau, S. Cea, T. Ghani, G. Glass, T. Hoffman, C. H. Jan, C. Kenyon, J. Klaus, K. Kuhn, Z. Ma, B. Mcintyre, K. Mistry, A. Murthy, B. Obradovic, R. Nagisetty, P. Nguyen, S. Sivakumar, R. Shaheed, L. Shifren, B. Tufts, S. Tyagi, M. Bohr, and Y. El-Mansy, "A 90-nm logic technology featuring strained-silicon," IEEE Trans. Electron Devices 51, 1790 (2004).
- ²²S. Pidin, T. Mori, K. Inoue, S. Fukuta, N. Itoh, E. Mutoh, K. Ohkoshi, R. Nakamura, K. Kobayashi, K. Kawamura, T. Saiki, S. Fukuyama, S. Satoh, M. Kase, and K. Hashimoto, "A novel strain enhanced CMOS architecture using selectively deposited high tensile and compressive silicon nitride films," *IEDM Technical Digest. IEEE International Electron Devices Meeting* (IEEE, 2004), pp. 213–216.
- ²³G. Tsutsui, S. Mochizuki, N. Loubet, S. W. Bedell, and D. K. Sadana, "Strain engineering in functional materials," AIP Adv. 9, 030701 (2019).
- ²⁴T. Peña, S. A. Chowdhury, A. Azizimanesh, A. Sewaket, H. Askari, and S. M. Wu, "Strain engineering 2D MoS₂ with thin film stress capping layers," 2D Mater. 8, 045001 (2021).
- ²⁵A. Azizimanesh, T. Peña, A. Sewaket, W. Hou, and S. M. Wu, "Uniaxial and biaxial strain engineering in 2D MoS₂ with lithographically patterned thin film stressors," Appl. Phys. Lett. 118, 213104 (2021).

- ²⁶T. Peña, A. Azizimanesh, L. Qiu, A. Muhkerjee, A. N. Vamivakas, and S. M. Wu, "Temperature and time stability of process-induced strain engineering on 2D materials," J. Appl. Phys. 131, 024304 (2022).
- ²⁷S. A. Chowdhury, K. Inzani, T. Peña, A. Dey, S. M. Wu, S. M. Griffin, and H. Askari, "Mechanical properties and strain transfer behavior of molybdenum ditelluride (MoTe₂) thin films," J. Eng. Mater. Technol. 144, 011006 (2021).
- ²⁸T. Peña, J. Holt, A. Sewaket, and S. M. Wu, "Ultrasonic delamination based adhesion testing for high-throughput assembly of van der Waals heterostructures," J. Appl. Phys. 132, 225302 (2022).
- ²⁹J. E. Lee, G. Ahn, J. Shim, Y. S. Lee, and S. Ryu, "Optical separation of mechanical strain from charge doping in graphene," Nat. Commun. 3, 1024 (2012).
- ³⁰A. Michail, N. Delikoukos, J. Parthenios, C. Galiotis, and K. Papagelis, "Optical detection of strain and doping inhomogeneities in single layer MoS₂," Appl. Phys. Lett. 108, 173102 (2016).
- ³¹V. Carozo, C. M. Almeida, B. Fragneaud, P. M. Bedê, M. V. O. Moutinho, J. Ribeiro-Soares, N. F. Andrade, A. G. Souza Filho, M. J. S. Matos, B. Wang, M. Terrones, R. B. Capaz, A. Jorio, C. A. Achete, and L. G. Cançado, "Resonance effects on the Raman spectra of graphene superlattices," Phys. Rev. B 88, 085401 (2013).
- ³²V. Carozo, C. M. Almeida, E. H. M. Ferreira, L. G. Cancado, C. A. Achete, and A. Jorio, "Raman signature of graphene superlattices," Nano Lett. 11, 4527–4534 (2011).
- 33A. Jorio and L. G. Cançado, "Raman spectroscopy of twisted bilayer graphene," Solid State Commun. 175–176, 3–12 (2013).
- 34A. E. Ennos, "Stresses developed in optical film coatings," Appl. Opt. 5(1), 51–61 (1966).
- 35 M. E. Thomas, M. P. Hartnett, and J. E. McKay, "The use of surface profilometers for the measurement of wafer curvature," J. Vac. Sci. Technol. A 6, 2570–2571 (1988).

- ³⁶G. C. A. M. Janssen, M. M. Abdalla, F. van Keulen, B. R. Pujada, and B. van Venrooy, "Celebrating the 100th anniversary of the Stoney equation for film stress: Developments from polycrystalline steel strips to single crystal silicon wafers," Thin Solid Films 517, 1858–1867 (2009).
- ³⁷C. Androulidakis, E. N. Koukaras, J. Partenios, G. Kalosakas, K. Pagagelis, and C. Galiotis, "Graphene flakes under controlled biaxial deformation," Sci. Rep. 5, 18219 (2016).
- ³⁸I. D. Wolf, "Micro-Raman spectroscopy to study local mechanical stress in silicon integrated circuits," Semicond. Sci. Technol. 11, 139 (1996).
- ³⁹T. M. G. Mohiuddin, A. Lombardo, R. R. Nair, A. Bonetti, G. Savini, R. Jalil, N. Bonini, D. M. Basko, C. Galiotis, N. Marzari, K. S. Novoselov, A. K. Geim, and A. C. Ferrari, "Uniaxial strain in graphene by Raman spectroscopy: G peak splitting, Grüneisen parameters, and sample orientation," Phys. Rev. B 79, 205433 (2009).
- ⁴⁰A. Dey, S. A. Chowdhury, T. Peña, S. Singh, S. M. Wu, and H. Askari, "An atomistic insight to the moiré reconstruction in twisted bilayer graphene beyond the magic angle," ACS Appl. Eng. Mater. 1, 970–982 (2023).
- ⁴¹D. E. Parker, T. Soejima, J. Hauschild, M. P. Zaletel, and N. Bultinck, "Strain-induced quantum phase transitions in magic-angle graphene," Phys. Rev. Lett. 127, 027601 (2021).
- ⁴²L. Zhang, Y. Wang, R. Hu, P. Wan, O. Zheliuk, M. Liang, X. Peng, Y.-J. Zeng, and J. Ye, "Correlated states in strained twisted bilayer graphenes away from the magic angle," Nano Lett. 22, 3204–3211 (2022).
- ⁴³F. Mesple, A. Missaoui, T. Cea, L. Huder, F. Guinea, G. T. de Laissardière, C. Chapelier, and V. T. Renard, "Heterostrain determines flat bands in magic-angle twisted graphene layers," Phys. Rev. Lett. 127, 126405 (2021).
- ⁴⁴Z. Bi, N. F. Q. Yuan, and L. Fu, "Designing flat bands by strain," Phys. Rev. B 100, 035448 (2019).